Electric Power Systems Research 106 (2014) 142–150

Contents lists available at ScienceDirect

Electric Power Systems Research

journal homepage: www.elsevier.com/locate/epsr

Probabilistic estimation of voltage sags using erroneous measurement information

N.C. Woolley[a], M. Avendaño-Mora[a], A.P. Woolley[b], R. Preece[a], J.V. Milanović[a,*]

[a] School of Electrical & Electronic Engineering, The University of Manchester, Manchester M60 1QD, UK
[b] London, UK

ARTICLE INFO

Article history:
Received 4 March 2013
Received in revised form 30 July 2013
Accepted 31 July 2013
Available online 19 September 2013

Keywords:
Distribution networks
Monitoring
Power quality
Voltage sags

ABSTRACT

Estimating voltage sag performance is important for distribution network operators who are keen to reduce costly interruptions, plan network investment and reduce operational expenditure. This paper proposes a robust method to locate faults and estimate the magnitude of voltage sags using information from a limited set of arbitrarily accurate monitoring devices. The developed method uses statistical analysis and impedance based fault location equations to find the most likely fault location and sag magnitude at non-monitored busbars. The method robustly handles measurement errors, and helps to eliminate some of the sensitivity present in existing impedance based fault location algorithms. The method is also shown to be effective at eliminating multiple fault location solutions caused by multiple overlapping impedance paths by synthesizing information from all monitors installed in a network. The method is validated and shown to be effective on a generic section of the UK's distribution network.

1. Introduction

Voltage sags represent the most significant component of power quality (PQ) problems in distribution networks [1] both in terms of gross numbers of events and the high associated costs to end users [2–4]. An EU study estimated that voltage sags and short interruptions contributed to an annual cost of €86bn [5] and in 2008/2009, voltage sags (and faults) caused an average of 0.73 interruptions per customer and contributed to an average of 76 customer minutes lost (CMLs) over the course of a one year period. These interruptions cause different impacts to different customers. For example, a momentary interruption for a large customer is estimated to cost £216k, whereas a 4 h interruption on a residential customer is estimated to cost only £4.78 [6].

Voltage sag performance estimation concerns both localizing the source of a voltage sag (most often a fault) and estimating the voltage sag magnitude in order to subsequently assess the impact on customers. DNOs are placing increasing emphasis on power quality monitoring to obtain greater visibility of power quality events, such as voltage sags, [7] beyond monitoring a limited group of large important customers. Through network wide monitoring, the level of power quality within a network can be quantified in terms of both events and costs and important current problems can be identified. Monitoring allows a DNO to perform reliability benchmarking, monitor power quality contracts and plan predictive maintenance [8]. Significant efforts in surveying power quality are also evidenced in the Benchmarking Report on the Quality of Electricity Supply of the Council of European Energy Regulators (CEER) [9]. A network operator's monitoring investment decision is also driven by other factors such as new initiatives like the Smart Grid, changes in the regulatory environment, concerns about customer retention and new competition within the utility sector. The Electric Power Research Institute (EPRI) lists forecasting and short circuit analysis as the two main reasons for monitoring alongside permanent power quality monitoring [8] in future power networks.

Finding the source of a voltage sag is closely related to the task of fault localization. This topic has been covered in existing research, recently in [10–14]. Fault localization in modern distribution networks is complicated in practice because information is only available from a limited number of variably accurate monitors. One of the most notable works which deals with measurement error is [13]. In [13] the authors developed a technique capable of locating faults using measurements taken from any two locations in the power network by utilizing an optimal estimation procedure based on the method of least squares. However, [13] does not consider how information from multiple monitoring devices could be combined to yield a distribution (rather than a point estimate) for the most likely fault location and does not consider situations where the number of monitors is fewer than required to obtain a single unique fault location estimate.

Estimating a fault-induced voltage sag's magnitude can be accomplished after the fault location has been identified. This two step procedure was implemented in [14]. Like [13], the approach

* Corresponding author. Tel.: +44 0161 306 8724; fax: +44 161 306 4820.
E-mail address: milanovic@manchester.ac.uk (J.V. Milanović).

0378-7796/$ – see front matter © 2013 Elsevier B.V. All rights reserved.
http://dx.doi.org/10.1016/j.epsr.2013.07.021

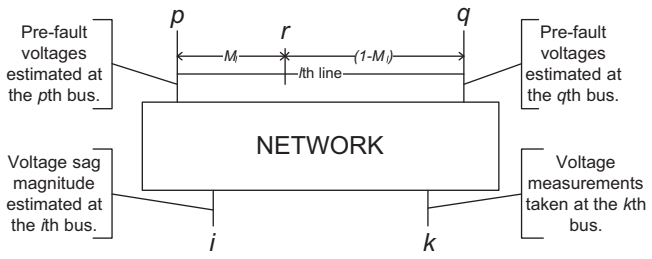

Fig. 1. A representation of the estimated and monitored buses required to perform fault location and voltage sag profile estimation.

taken in [14] yields a single estimate for an output parameter, in this case voltage sag magnitude. An alternative to voltage magnitude estimation is to simulate a short circuit fault at the fault location identified [15,16].

The method developed in this paper adds to the research developed in [11,13] and has several advantages over existing techniques. It firstly allows power system operators to formulate a robust statistical estimate for both the fault location and voltage sag profile whilst taking into account the errors of monitoring devices within the network. Secondly, the method is independent of the accuracy of the monitoring device, so operators can utilize measurements from any monitoring device available in their network, including relays, power quality meters, disturbance recorders, phasor measurement devices (PMUs) or revenue meters. Lastly, the method synthesizes a fault location using all available information from an arbitrary positive number of devices. By using information from all available monitors, both the fault location and voltage profile estimate are more accurate than the single or double ended approaches presented in [11]. It also overcomes some issues caused by multiple impedance paths by reducing the number of fault locations to those that are the most feasible.

2. Impedance based fault localization and sag magnitude estimation

Impedance based fault location algorithms [11] utilize the impedance of the network and the observed voltage drop to arrive at an estimated fault location. Impedance based methods may be transient, or steady state, and typically use measurements from monitors at one or both ends of a line. This research advances the steady state single monitor impedance based algorithms developed in [11]. The algorithm presented in this paper extends the approach described in [11], enabling one, two or any number measurements taken anywhere in a network to be synthesized into a single fault location estimate.

The equations developed in [11] calculate the fault location using measured data from one or two monitoring devices. The equations require pre-fault voltage measurements at the monitored bus and at the ends of the faulted line, as well as during-fault voltage measurements at the monitored busbar. The equations are also independent of fault impedance, if the fault impedance is assumed to be entirely resistive [11].

2.1. Fault localization equations

The aim of the fault localization equations can be illustrated through Fig. 1. The objective of the equations is to locate a fault at position r along the lth line between buses p and q and then subsequently perform voltage sag profile estimation at a non-monitored bus i with measurements taken at the kth busbar.

Assuming the network's impedance parameters can be derived accurately, the accuracy of the fault location equations will depend upon the values of the measured pre-fault voltages at the kth busbar and the estimated pre-fault voltage at the ends of the lth line. The accuracy of the measurement at the kth busbar is dependent on the installed monitor's accuracy, and this may vary depending on the device that is installed. Unless there happens to be a monitor at either the pth or the qth busbar, these voltages must be estimated through distribution system state estimation (DSSE) [17]. The accuracy of the DSSE voltage estimates will directly depend on the accuracy of the pseudo-measurements used to estimate the load throughout the network.

2.1.1. Single line to ground (SLG) faults

The fault location equation for a SLG fault is shown in Eq. (1).

$$M_l = \frac{B_k^{(2)} - G_k B_k^{(0)}}{G_k C_k^{(0)} - C_k^{(2)}} \tag{1}$$

where $B_k^{(i)}$ and $C_k^{(i)}$ are network dependent parameters and are derived from elements in the $\boldsymbol{Z_{bus}}$ impedance matrix, G_k is the ratio of the negative sequence voltage to the zero sequence voltage $(E_k^{(2)}/E_k^{(0)})$ as measured at bus k and M_l is the distance in per unit along the faulted line l [11]. Note that the derivation of $B_k^{(i)}$ and $C_k^{(i)}$ are not shown here for brevity, but this is covered in detail (using the same notation) in [11].

For SLG faults, M_l can be solved independently of fault impedance and pre-fault voltage estimates. The accuracy of M_l is dependent only on the accuracy of during-fault measurements at the monitored bus k ($E_k^{(2)}$ and$E_k^{(0)}$).

Similar single monitor fault location equations can be derived for line to line, double line to ground, and three phase symmetrical faults. Full sets of equations can be found in [11].

2.1.2. Calculating voltage sag depth

The calculated values of the fault location M_l can be used to determine the during-fault voltage drops at the ith unmonitored busbar. The during-fault voltage drops at bus i can be considered as functions of the fault location and the measured voltage at bus k only. These during-fault voltage drops in the sequence domain are expressed in Eqs. (2)–(4):

$$E_i^{(0)(k)} = \frac{Z_{ir}^{(0)} E_k^{(0)}}{Z_{kr}^{(0)}} = E_k^{(0)} \frac{B_i^{(2)} + C_i^{(2)} M_l}{B_k^{(2)} + C_k^{(2)} M_l} \tag{2}$$

$$\begin{aligned} E_i^{(1)(k)} - E_i^{(1)0} &= -\frac{Z_{ir}^{(2)} (E_k^{(1)0} - E_k^{(1)})}{Z_{kr}^{(1)}} \\ &= (E_k^{(1)0} - E_k^{(1)}) \frac{B_i^{(1)} + C_i^{(1)} M_l}{B_k^{(1)} + C_k^{(1)} M_l} \end{aligned} \tag{3}$$

$$E_i^{(2)(k)} = \frac{Z_{ir}^{(2)} E_k^{(2)}}{Z_{kr}^{(2)}} = E_k^{(2)} \frac{B_i^{(2)} + C_i^{(2)} M_l}{B_k^{(2)} + C_k^{(2)} M_l} \tag{4}$$

Note that the superscript (k) denotes that $E_i^{(s)(k)}$ the voltage at bus i is calculated from measurements taken at the kth monitor (where s denotes the sequence). $E_i^{(s)0}$ is the pre-fault voltage as measured at the kth (monitored) busbar. Eqs. (2)–(4) are independent of pre-fault voltage estimates and fault impedance. However, M_l may be dependent on pre-fault voltage estimates and fault impedance, subject to the fault type.

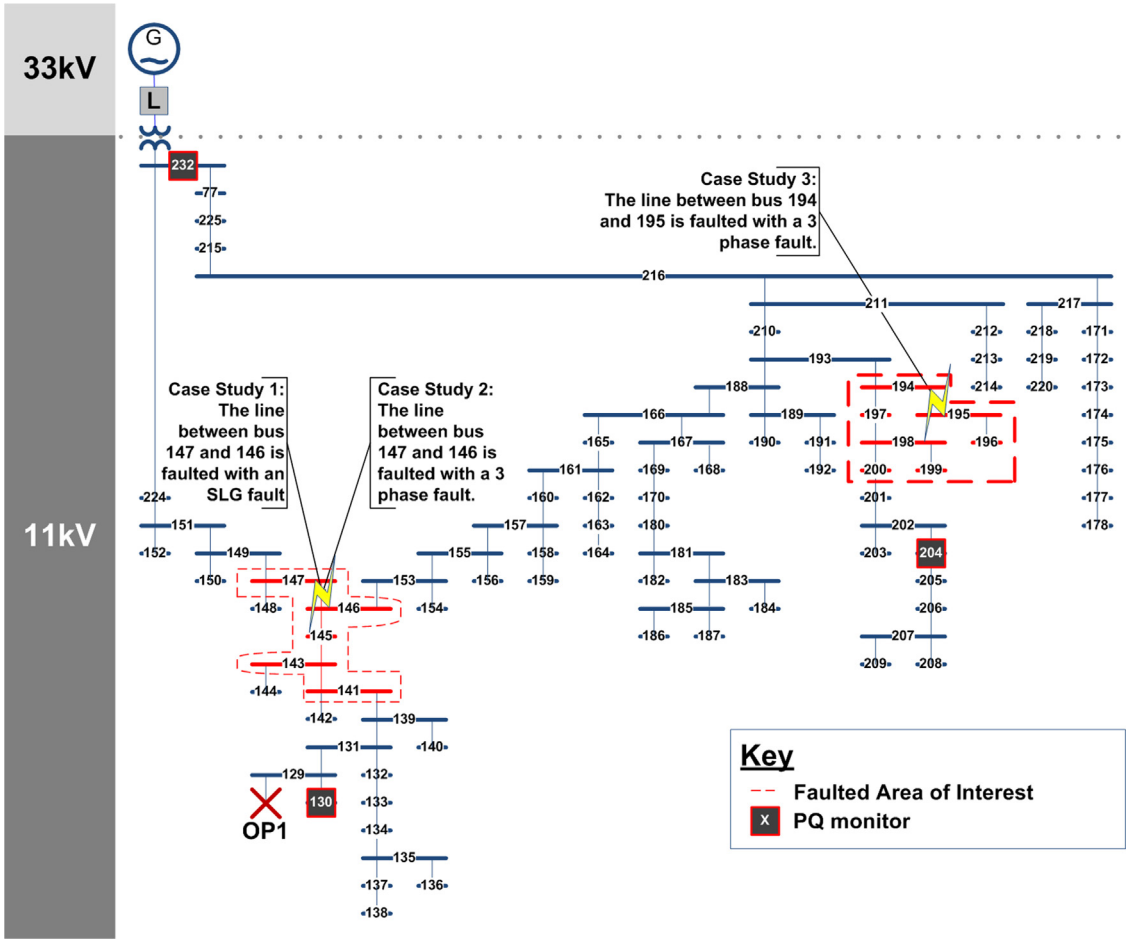

Fig. 2. 94 Bus section of a 295 bus generic distribution network [22].

3. Uncertain quantities in the fault localization equations

3.1. Errors in measured voltages

The fault localization equations use measurements from monitoring devices which may be subject to errors. The accuracy of the measurement will vary depending on the quality of the monitoring device [18]. Monitor measurement errors can be modeled as a series of independent normal distributions [19]. Given a calibrated percentage error for a monitoring device (*%error*), a monitor's error is modeled as a normal distribution. An error of 0.2% of the true value was assumed for all symmetrical component magnitudes and 0.2% of 2π for phase measurements [18] (where 0.2% is equal to 3 standard deviations). The standard deviation for the voltage magnitude and phase was therefore $\sigma_{|E|} = 0.067\%$ and $\sigma_{\varphi} = 0.0013\pi$ radians, respectively [19].

Errors are assumed to be zero-mean, therefore the mean of the voltage magnitude and phase at the kth busbar are the measured values, $|\bar{E}_k^{(s)}|$ and $\bar{\varphi}_k^{(s)}$ (for an arbitrary sequence s). Eqs. (5) and (6) define the probability distributions of a measurement at the kth bus in an arbitrary sequence s. Both $|E_k^{(s)}|$ and $\phi_k^{(s)}$ are assumed to be independent.

$$|E_k^{(s)}| \sim N(|\bar{E}_k^{(s)}|, \quad \sigma_{|E_k|}) \tag{5}$$

$$\varphi_k^{(s)} \sim N(\bar{\varphi}_k^{(s)}, \quad \sigma_{\varphi k}) \tag{6}$$

3.2. Errors in pre-fault voltage estimates

Pre-fault voltages can either be obtained by direct measurement if a monitor is present, or by estimating the voltage using DSSE [17]. If direct measurement is used, the errors in voltage measurements were assumed to be distributed as defined by Eqs. (5) and (6).

Physical measurement inputs to the DSSE were modeled using the measurement model described by Eqs. (5) and (6), assuming independence between monitoring devices. Pseudo-measurement inputs were modeled by assuming that the value of the real and reactive power injection (load) at each busbar can be estimated based on historical knowledge of the load profile. A percentage error of 20% (equal to 3σ) was selected for all load estimation pseudo-measurements [20].

The accuracy of the pre-fault voltage estimates obtained using DSSE can be illustrated using a simple example. The standard deviation for pseudo-measurements was set as described and the standard deviation of real measurements was set to 0.2%, with both assumed to follow a normal distribution. Using the three monitors as shown in Fig. 2, the maximum standard deviation for the voltage magnitude of a non-monitored bus ranges between 1.5% and 4.3% of the true voltage magnitude. This defines the accuracy of the pre-fault voltage estimates which will be used as inputs to the fault location equations.

The fault localization equations are also sensitive to variation in network impedance parameter errors. Network impedances were assumed to be free from error.

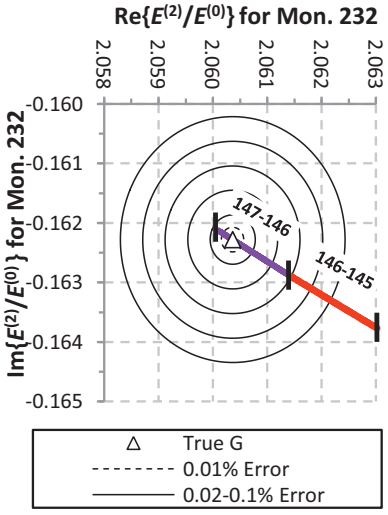

Fig. 3. Contours of constant G_{232} for errors in $|E^{(2)}_{232}|$ and $|E^{(0)}_{232}|$.

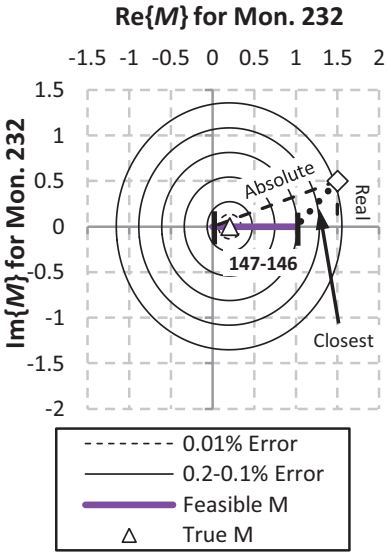

Fig. 4. The range of true and erroneous solutions for $M_{147\text{-}146}$ given a constant error in $|E^{(2)}_{232}|$ and $|E^{(0)}_{232}|$.

4. Difficulties using the single monitor fault localization equations

The fault localization equations are extremely powerful, but they introduce difficulties when used in a practical monitoring deployment. A general difficulty with fault localization and sag magnitude estimation arises when the set of monitors being used to calculate a fault location is not able to observe all the voltages within the network. In this scenario, multiple fault location solutions can be found where the same sets of voltages and currents can be observed for multiple locations within the network [21]. References [12] and [14] tackled this issue by estimating the fault location as the intersection of several monitors' fault location estimates. There is no guidance however for how close fault locations should be before they are considered to overlap.

The equations also involve complex numbers and therefore if any of the measurements are slightly erroneous, the fault location may be two dimensional. The work presented in [11] does not provide guidance on how to deal with complex solutions, which often arise if measurements are slightly in error.

One of the most important issues with the fault location equations is their sensitivity to small changes in input measurements. Small errors in inputs to the equations may result in large changes in the estimated output, and solutions to the equations which may diverge into the complex plane.

4.1. Sensitivity of the equations to uncertainty

The sensitivity of the equations can be demonstrated by considering an example. Fig. 2 shows a section of a generic 295 bus distribution network (adapted from [22,23]), with feeder L highlighted. Consider the situation where a single monitor is installed at bus 232 which observes a single phase to ground fault in phase A between buses 147 and 146 (with zero fault resistance) at a distance of 0.206 per unit from bus 147. During the fault, the voltages at bus 232 drop to 0.62, 0.94 and 0.98 per unit in phases A, B and C, respectively.

Fig. 3 shows contour lines representative of introducing a constant percentage error in the zero or negative sequence voltage magnitude only. The figure also shows valid values for G_{232} (where the value of M_l in Eq. (1) is between 0 and 1 and not complex) along lines connecting buses 147 to 146 and 146 to 145.

Fig. 3 highlights that even a small error of 0.1% in a magnitude measurement could lead to the fault location solution being assigned to the incorrect line. To localize this fault within 10% of the length of the line, a monitor at 232 would need to be accurate to within 0.01% of the true voltage magnitude (unrealistic for a distribution network monitor).

Fig. 4 shows how these errors map into solutions for $M_{147\text{–}146}$ using Eq. (1). The diamond point in Fig. 4 illustrates the difficulty of formulating a solution for $M_{147\text{–}146}$ based on erroneous measured voltages. The example solution (M_e) is only in error by 0.1%, but the solution to the fault location equations is now complex. A basic estimate for the fault location could be achieved by either taking the real part of M_e (Re$\{M_e\}$, as used in [12]) or the magnitude of M_e ($|M_e|$). Both of these methods result in solutions which are greater than 1 (1.5 for Re$\{M_e\}$ and 1.58 for $|M_e|$). Thus it would be incorrectly concluded that the fault did not occur on the line. A more advanced and realistic approach would be to consider the possibility that the measurement was erroneous, and predict a fault location given a known measurement error distribution. In Fig. 4 a dotted line (labeled "closest") shows most likely position for the fault ($M_e = 1$) which maps M_e to the closest point on the valid line of solutions for $M_{147\text{–}146}$.

There are two problems which are shown by this brief analysis. Firstly, it is clear that the fault location equations are highly sensitive to even small measurement errors. If measurement error cannot be robustly eliminated, this will limit the usefulness of an impedance based approach. Secondly, when the fault location equations are subjected to small errors they generate complex solutions. Although the only physically meaningful solutions for Eq. (1) are real, it is also important to consider the likelihood of a complex solution given some measurement error.

It should be noted that the examples in Figs. 3 and 4 are purposely simplistic to aid illustration; the analysis only considers variation in one dimension, namely zero or negative sequence voltage magnitude. In practice, the magnitude and/or phase of all voltages may be in error, thus creating a more complicated four dimensional error space.

5. A probabilistic approach to fault localization and voltage sag magnitude estimation

The problems with the fault localization equations can be successfully minimized by extending them to incorporate the statistical properties of measurement errors. A probabilistic approach

means that fault locations are converted from discrete points into distributions, therefore identifying the *most likely* fault location and the *best estimate* for the voltage sag magnitude.

5.1. Probabilistic fault localization

The aim of probabilistic fault localization is to find a probability density function (PDF) (f_F) for the fault location F, conditional that a fault occurred on a line within the network. To estimate a fault location for a given fault type, the fault location equations are solved for each of the lines in the network. Solutions at customer sites are not considered.

Solving the fault location equations yields a solution for M_l: the location of the fault along the lth line. The values of M_l which are physically meaningful are located on the real axis, between 0 and 1. Errors in the fault location equation's variables may cause M_l to move off the real axis and into the complex plane. Note that a fault at a busbar is equivalent to a value of M_l equal to 0 or 1, and is thus covered by considering fault location solutions in the range [0,1].

It should be noted that M_l is a random variable because it is a function of erroneous voltage measurements and estimates. At an arbitrary point m_l along the lth line, for a specific monitor k, the kth monitor's measurement errors (and the errors of estimates performed using DSSE) can be used to define the probability distribution of M_l as $f_{M_l^{(k)}}(m_l^{(k)})$.

If it is noted that $f_{M_{l_j}}(m_{l_j})$ is only of interest where m_l is real and between 0 and 1, the distribution of M_l can be re-written as a conditional distribution as shown in Eq. (7).

$$f_{M_l}^{[0,1]}(m_l) = f_{M_l}(m_l | M_l \in [0,1]) = \frac{f_{M_l}(m_l)}{\int_{\Re_{[0,1]}} f_{M_l}(m_l)dm_l} \forall m_l \in [0,1] \quad (7)$$

where $\Re_{[0,1]}$ is a line in the complex plane along the real axis between 0 and 1. Eq. (7) therefore describes the probability distribution for the fault location along the lth line conditional that the fault occurred along the lth line in the network.

Eq. (7) can be extended to a multi-line system to find the PDF for the fault location M_l on a specific line l contained within a set of all lines L ($l \in L$).

$$f_{M_{l_j}}^{[0,1]}(m_{l_j}) = \frac{f_{M_{l_j}}(m_l)}{\sum_{l_i \in L} \int_{\Re_{[0,1]}} f_{M_{l_i}}(m_{l_i})dm_{l_i}} \forall m_{l_j} \in [0,1] \quad (8)$$

$$\sum_{l_j \in L} \int_0^1 f_{M_{l_j}}^{[0,1]}(m_{l_j}) = 1 \quad (9)$$

$$f_F = \left\{ f_{M_{l_1}}^{[0,1]}(m_{l_1}), \quad f_{M_{l2}}^{[0,1]}(m_{l_2}), \ldots, \quad f_{M_{l_N}}^{[0,1]}(m_{l_N}) \right\} \quad (10)$$

$$f_F^{(k)} = \left\{ f_{M_{l_1}^{(k)}}^{[0,1]}(m_{l_1}^{(k)}), \quad f_{M_{l_2}^{(k)}}^{[0,1]}(m_{l_2}^{(k)}), \ldots, \quad f_{M_{l_N}^{(k)}}^{[0,1]}(m_{l_N}^{(k)}) \right\} \quad (11)$$

Eq. (8) describes the PDF that the fault location, F, is found on the lth line specifically. Eq. (10) shows a continuous set of functions (for all the lines in the network) which together describe the PDF of the fault location. In Eq. (11), $f_F^{(k)}$ describes the PDF for the fault location using one specific monitor k.

5.2. Probabilistic estimation of voltage sag magnitude

Voltage sag magnitude estimation is accomplished by calculating the voltage at a non-monitored bus i using Eqs. (2)–(4). The voltage sag magnitude estimation equations calculate sequence voltages ($E_i^{(0)(k)}$, $E_i^{(1)(k)}$ and $E_i^{(2)(k)}$) which can be transformed into phase voltages by applying the Fortescue transformation. The aim is to calculate the distribution of the magnitude of the phase voltages ($|E_i^{(a)(k)}|$, $|E_i^{(b)(k)}|$ and $|E_i^{(c)(k)}|$), $f_{|E_i^{(j)(k)}|}(|e_i^{(j)(k)}|)$, where $j \in \{a, b, c\}$.

Since each monitor is independent, a multivariate probability distribution can be formed for the voltage magnitude at the ith bus as shown in Eq. (12).

$$f_{M_l^{(1)}M_l^{(2)}\ldots M_l^{(N)}}(m_l^{(1)} \cdot m_l^{(2)} \cdot \ldots \cdot m_l^{(3)}) = f_{M_l^{(1)}}(m_l^{(1)}) \cdot f_{M_l^{(2)}}(m_l^{(2)}) \cdot \ldots \cdot f_{M_l^{(N)}}(m_l^{(N)}) = f_{M_l}(m_l) \quad (12)$$

$$f_{|E_i^{(s)(1)}|\cdots|E_i^{(s)(N)}|}(|e_i^{(s)(1)}|, \ldots, |e_i^{(s)(N)}|) = f_{|E_i^{(s)(1)}|}(|e_i^{(s)(1)}|) \times \cdots \times f_{|E_i^{(s)(1)}|}(|e_i^{(s)(N)}|) = f_{|E_i^{(s)}|}(|e_i^{(s)}|) \quad (13)$$

The PDF $f_{|E_i^{(s)}|}(|e_i^{(s)}|)$ describes the voltage magnitude at the ith bus in the sth sequence estimated using information from all of the monitors within the network.

5.3. PDFs for the fault location and voltage sag magnitude

The PDF distribution of f_F and $f_{|E_i^{(j)}|}(|e_i^{(j)}|)$ can be estimated through a Monte Carlo simulation with non-parametric kernel density estimation [24]. For each monitor, a Monte Carlo simulation is run by drawing zero, positive and negative sequence voltages from the distributions shown in Eqs. (5) and (6). For each busbar where the voltage was estimated using DSSE, voltages are obtained by running DSSE with pre-fault input measurements and pseudo-measurements drawn from the distributions shown in Eqs. (5) and (6) whilst selecting the appropriate standard deviation.

5.3.1. PDFs for the fault location

Each time the voltages are drawn, the fault location equations are solved. This generates a set of fault location estimates for each of the monitors in the network. Although the fault location solution should always be between 0 and 1, it is mathematically possible (and indeed likely) that the solution may be complex, exceed the bounds of 0 to 1 or be found in multiple positions on the same or other line. In the case where a monitor's set of solutions are not entirely real, the PDF can be estimated using bivariate kernel density estimation [24]. If the solutions are entirely real, kernel density estimation in a single dimension will suffice. The total PDF for the fault location, f_F, can be calculated by multiplying together the kernel density estimated PDFs for all of the monitors.

5.3.2. PDFs for the voltage sag profile magnitude

The PDF of the voltage magnitude at the ith bus, in the jth phase, measured by the kth monitor, across all lines, $f_{|E_i^{(j)(k)}|}(|e_i^{(j)(k)}|)$ can be found by using the results of fault location. Firstly, the PDF of the fault location, $f_{M_L^{(k)}}^{[0,1]}(m_l^{(k)})$, is used to generate values of $M_l^{(k)}$ by selecting random values from this distribution. Next, during-fault voltages $E_k^{(s)(k)}$ and pre-fault voltages $E_k^{(s)(k)'}$ are generated by selecting random numbers using Eqs. (5) and (6). Thirdly, the selected values are used to compute a set of during-fault voltage estimates using Eqs. (2)–(4). Lastly, a PDF can be estimated by using bivariate kernel density estimation. The combined PDF for the voltage sag profile (in the jth phase), $f_{|E_i^{(j)}|}(|e_i^{(j)}|)$, can be calculated by

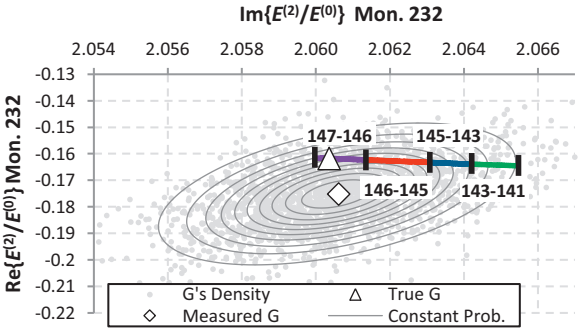

Fig. 5. The range of expected values for G_{232}.

multiplying together the kernel density estimated PDFs for all of the monitors.

6. Case studies

A section of the 295 bus distribution network was used to illustrate the concept of probabilistic fault localization and voltage sag magnitude estimation. Fig. 2 shows the section of network chosen. It covers a total of 94 busbars connected to feeder L.

Three monitors were assumed to be installed in the network, with locations corresponding to a subset of the optimal monitoring locations found through monitor placement optimization [23]. It should be noted that the positions of monitors for this study are not important; the probabilistic fault location method could be applied to any arbitrary set of monitors. All the monitors were assumed to measure three phase voltage magnitude, real and reactive power.

Three fault case studies were chosen: (1) a single line to ground (SLG) fault between buses 147 and 146, (2) a three phase fault between buses 147 and 146, and (3) a three phase fault between buses 194 and 195. All three faults were simulated at $m = 0.206$ along the line. Fig. 2 shows the location of all three case studies.

The aim of the first two case studies is to predict the voltages at buses 141, 143, 145, 146 and 147 during the fault. Table 1 shows the true during-fault voltages for both case studies at each of these 5 buses. The aim of the third case study is to show how the proposed probabilistic approach to fault localization helps to eliminate multiple fault location estimates.

6.1. Case study 1: SLG fault between buses 147 and 146

For the SLG fault, the key parameter in Eq. (1) is G, the ratio of $E^{(2)}/E^{(0)}$. Fig. 5 shows a plot of the distribution of G_{232} produced from its true value (at $M_{232} = 0.206$) and the expected variation in G_{232} around this measured point. The contour lines represent lines of constant probability. The variation of M_l in the complex plan is represented by the sections of lines shown for each of four power lines of interest.

The probability distribution for the fault location $f_F^{(232)}$ is shown in Fig. 6. This is a 2-dimensional representation of the height of the contours in Fig. 5 as they cut through the G plane with different values of M_l along each of the 4 lines.

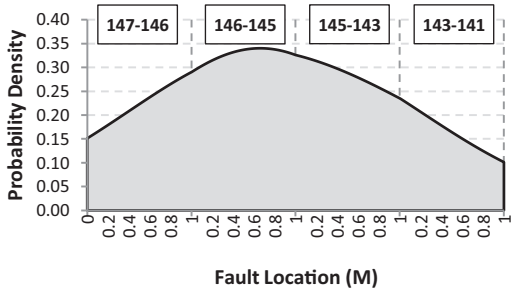

Fig. 6. The PDF for the fault location $f_F^{(232)}$.

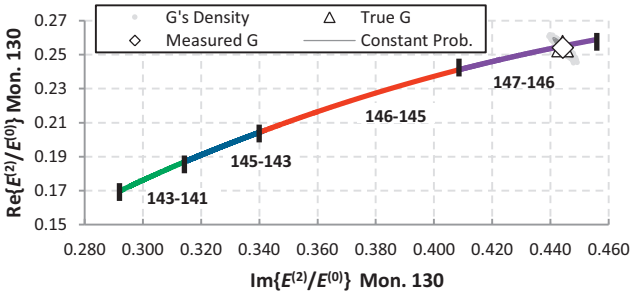

Fig. 7. The range of expected values for G_{130}.

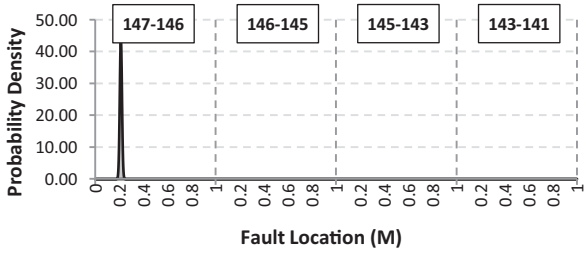

Fig. 8. The PDF of the fault location for a SLG fault: $f_F^{(130)}$ ($f_F^{(204)}$ follows a very similar profile).

Fig. 6 highlights that a monitor at bus 232 cannot accurately locate the fault between buses 147 and 146. Indeed, $f_F^{(232)}$ does not vary significantly across all of the lines, and the peak between buses 146 and 145 does not correspond to the true fault location. This evidence suggests that a monitor at bus 232 less accurately locates faults within this section of the network.

Figs. 7 and 8 show G_{130} and $f_F^{(130)}$ for a monitor placed at bus 130 while Fig. 9 shows G_{204} for a monitor placed at bus 204. The distribution of $f_F^{(130)}$ (and $f_F^{(204)}$) are now very tight, and the fault is accurately localized at $m_{232} = 0.206$ along the line between buses 146 and 147. The variation of the error in G_{130} and G_{204} relative to the solutions for G along the line connecting buses 147 to 146 is relatively small, and markedly different to the relative variation for

Table 1
During-fault voltages for case studies 1 and 2.

Bus	Case study 1: SLG fault between buses 147 and 146			Case study 2: 3 phase fault between buses 147 and 146		
	Phase A	Phase B	Phase C	Phase A	Phase B	Phase C
Bus 147	0.117	0.956	1.293	0.0122	0.0122	0.0122
Bus 146	0.129	0.956	1.305	0.0010	0.0010	0.0010
Bus 145	0.130	0.956	1.304	0.0006	0.0006	0.0006
Bus 143	0.130	0.956	1.303	0.0004	0.0004	0.0004
Bus 141	0.131	0.954	1.302	0.0002	0.0002	0.0002

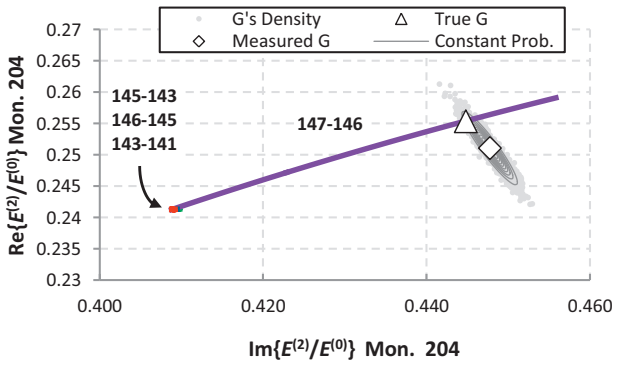

Fig. 9. The range of expected values for G_{204}.

bus 232. The error distribution for both G_{130} and G_{204} cuts the line at almost exactly $m = 0.2$. This implies that both of these monitors are good at locating faults at this point in the network.

Figs. 7 and 9 show that there is a significant difference between the solutions of G_{130} and G_{204} along the lines connecting buses 146 to 141. The monitor at bus 204 sees the lengths of these connections as negligibly short distances when compared to the length of the line connecting bus 147 to 146. In practical terms, this means a monitor placed at bus 204 will not be able to accurately localize faults between buses 146 and 141, or near to the end of the line connecting buses 147 to 146.

The probability distributions for the fault location were used to build a probability distribution for the voltage magnitude at each of the five monitored buses. Fig. 10 illustrates the shape of the estimated PDFs for the voltage in phase A at bus 146 using each of the three monitors individually ($f_{|E_{146}^{(a)(130)}|}$, $f_{|E_{146}^{(a)(204)}|}$ and $f_{|E_{146}^{(a)(232)}|}$) and the estimated PDF using all the monitors combined ($f_{|E_{146}^{(a)}|}(|e_{146}^{(a)}|)$). The PDF for all monitors is clearly more accurate than either of the individual monitors, narrowing in on the true value of 0.129 per unit. The inaccuracy in fault location using only a monitor at bus 232 is apparent in $f_{|E_{146}^{(a)(232)}|}$, whose distribution peaks at around 0.19 per unit, 0.06 per unit from the true during-fault voltage.

It can be concluded that combining the information from all four monitoring devices yields the best performance for estimating SLG faults. The monitor placed at bus 232 is the worst performing monitor for estimating SLG faults.

6.2. Case study 2: 3 phase fault between buses 147 and 146

Figs. 11 and 12 show the PDFs for the fault location using each monitor individually and all monitors together to locate the fault. The most accurate estimate for the fault location is obtained using data from a monitor placed at bus 232 whilst the least accurate

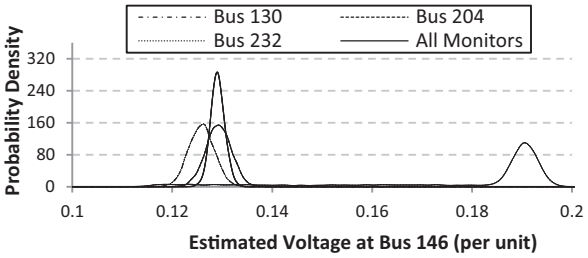

Fig. 10. The estimated probability distribution of the voltage magnitude in phase A at bus 146 using measurements from buses 130, 204, 232 and all buses combined for a single phase to ground fault.

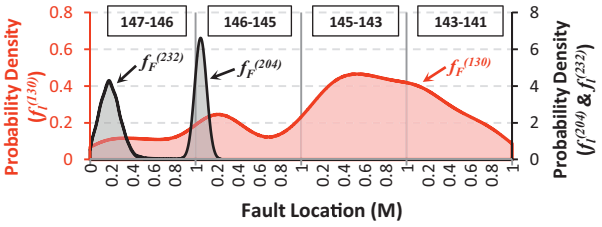

Fig. 11. The PDF of the fault location for a three phase fault: $f_l^{(130)}$, $f_l^{(204)}$, and $f_l^{(232)}$.

monitor estimate is formulated using data from a monitor at bus 130.

The shapes for each of the PDFs shown in Figs. 11 and 12 can be explained qualitatively by considering the network topology and monitor's location with respect to the fault. A three phase fault with zero fault resistance between buses 146 and bus 147 causes all phase voltages to drop to approximately zero downstream of the fault location. When solving for M_l using a monitor at bus 130 (Fig. 11), the sensitivity of Eq. (1) is increased and the fault location estimate is consequently uncertain.

Fig. 11 also shows that the solutions for m using a monitor at bus 204 yield solutions on both the line connecting buses 146 to 147 and the line connecting buses 146 to 145. This can be explained by noting bus 204's nearest connection to the network section of interest is via bus 146. Solving Eq. (10) yields two solutions, which both represent identical impedance paths between bus 204 and the fault location. The impedance of the line connecting buses 146 to 145 is over twice that of the line 146 to 147. This causes the $f_F^{(204)}$ to peak in Fig. 11 at approximately $m = 0.1$ along the line connecting buses 146 to 145. The PDF still correctly overlaps the true fault location on the line connecting buses 146 to 147 at $m = 0.206$, but the equation which governs the line connecting buses 146 to 147 is non-linear and sensitive such that Eq. (1) yields solutions outside of the length of the line, thus reducing the overall area of the PDF on the line.

Fig. 11 lastly shows the results of using a monitor at bus 232 to locate the fault. The PDF peaks at 0.2, and there are no aliased fault locations on other lines. Bus 232 is connected to the primary

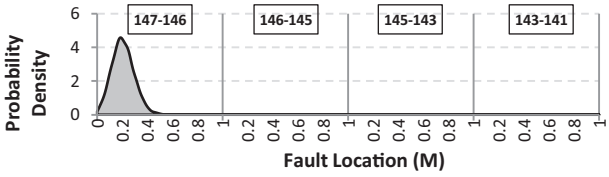

Fig. 12. The PDF of the fault location for a three phase fault: f_F.

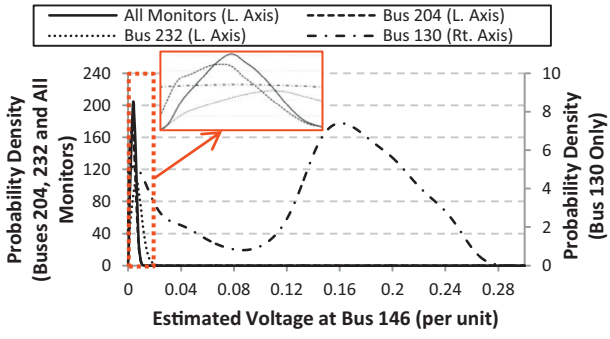

Fig. 13. The estimated probability distribution of the voltage magnitude in all three phases at bus 146 using measurements from buses 130, 204, 232 and all buses combined for a three phase fault. The inset shows a zoomed diagram of voltages less than 0.01 per unit.

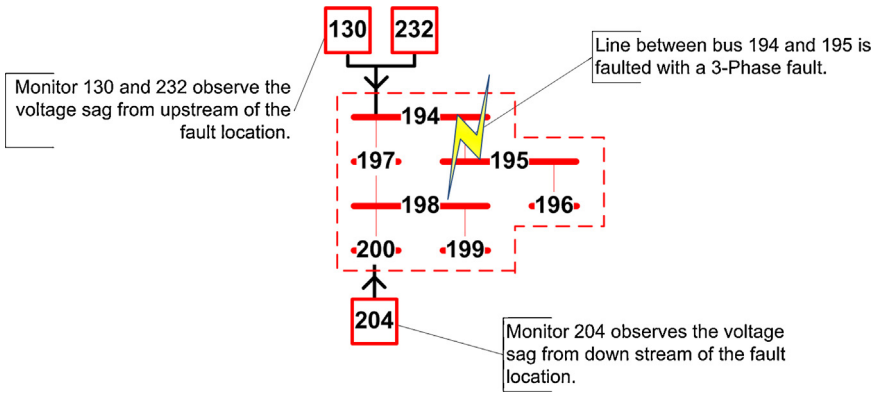

Fig. 14. A three phase fault simulated between buses 194 and 195. Monitors at buses 204, 130 and 232 observe the voltage sag.

in-feed for this area of the network, and is thus a relatively strong bus; it experiences a drop in voltage magnitude of 64% compared with the near 100% drop in voltage magnitude at bus 130. Eq. (1) is therefore relatively insensitive to errors in monitoring and an accurate estimate for the fault location can be calculated.

Fig. 13 shows the results of voltage sag profile estimation when using each of the monitors to estimate the voltage magnitude at bus 146. Using information from a monitor placed at bus 232 yields the best performance, with a monitor at bus 204 also correctly pinpointing the voltage within the 0–0.02 per unit range. Although the voltage profile predicted by a monitor at bus 130 covers a large range between 0 and 0.3 per unit, any of these voltages would definitely cause serious disruption to equipment attached to bus 146 and the error is therefore insignificant in practical terms. The difference becomes important at a certain threshold, which depends on a specific piece of equipment's immunity to voltage sags.

It is interesting to note that the best monitor at predicting the during-fault voltages for the 3 phase fault was a monitor at bus 232 and the worst performing monitor was bus 130. For the SLG fault, the opposite was true. This indicates that the best monitor location to estimate an SLG fault is not necessarily the same for a three phase fault.

6.3. Case study 3: eliminating multiple location estimates

The benefits of using the proposed method to identify a unique solution for the source of the voltage sag can be explored by considering a three phase fault simulated between buses 194 and 195 (as shown in Fig. 2). This section of network is shown in more detail in Fig. 14.

The PDF for each of the three monitors and the combined distribution of all three monitors is shown in Fig. 15. This shows that each of the three monitors predict that the fault could have occurred at multiple locations within the network. For example $f_F^{(130)}$ shows three peaks on the lines connecting buses 197 to 198, buses 194 to 197 and buses 194 to 195. The monitor at bus 130 observes the network upstream of the fault and sees two impedance paths beyond bus 194: one to bus 197 and one to bus 195 (see Fig. 14). The monitor at bus 130 cannot distinguish between these two paths, and this ambiguity is reflected in the multiple peaks of $f_F^{(130)}$. The result $f_F^{(232)}$ also shows ambiguity because it too observes multiple impedance paths upstream of the fault location. Fig. 15 also shows multiple peaks for $f_F^{(204)}$. This is caused because this monitor sees two similar impedance paths from bus 198 to bus 196 and from bus 198 to bus 199. The strength of the proposed technique at helping to eliminate multiple fault location solutions is highlighted in the combined graph for all monitors shown in Fig. 15. By using the information

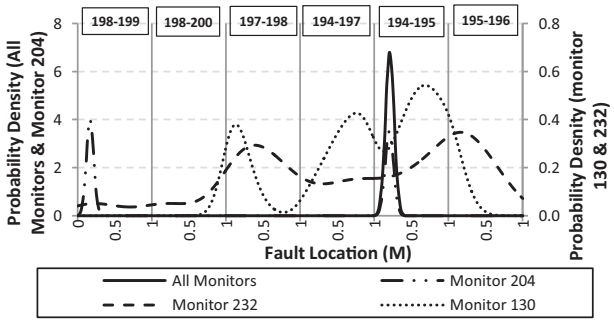

Fig. 15. The PDF across 6 lines for a three phase fault at 0.2 per unit along the line connecting bus 194 to bus 195 using all monitors (f_I), a monitor installed at bus 204 ($f_F^{(204)}$), 232 ($f_F^{(232)}$) and 130 ($f_F^{(130)}$).

available from all monitors, the PDF shows only one peak at the true fault location.

7. Conclusion

This paper presents a comprehensive method to identify a statistical distribution for both the fault location and the during sag voltage profile using only a small selection of arbitrarily accurate monitors. The method takes into account the potential variability of device measurements, and integrates relevant information from all monitoring devices in a network into a single statistical estimate. The method can be applied to three phase, SLG, line to line and double line to ground faults. Unlike existing deterministic techniques, the method formulates a statistical distribution for the fault location and voltage sag magnitude.

The research presented has several advantages over existing techniques. Some of the advantages of the method include: (i) the ability to work with any positive number of real monitors, i.e., there must be at least one monitor in the network; (ii) the ability to integrate the accuracy of monitors into a statistical estimate; (iii) the flexibility to add newer and more accurate monitoring devices; (iv) the capability to deal with the sensitivity of the fault location equations, (v) increased accuracy versus traditional single or double ended fault equations techniques by synthesizing information from more than two monitors; and (vi) the ability to eliminate multiple fault location estimates.

An extension of the research presented in this paper is to analyze the effects of network impedance uncertainties on fault localization and sag magnitude estimation. These uncertainties could be modeled using the approach defined in this paper for measurement uncertainties.

Acknowledgment

Thanks to Bob Ferris of Central Networks, Kate Grant and Rachel Stanley of E.ON New Build & Technology for their help and guidance on this project.

References

[1] Voltage Dip Evaluation and Prediction Tools, in: CIGRE Working Group C4.102 (2009).
[2] D. Chapman, The Cost of Poor Power Quality (November), Copper Development Association, 2001.
[3] M.H.J. Bollen, Understanding Power Quality Problems Voltage Sags and Interruptions, Wiley, Piscataway, 1999.
[4] J. Arrillaga, M.H.J. Bollen, N.R. Watson, Power quality following deregulation, Proc. IEEE 88 (2000) 246–261.
[5] R. Targosz, J. Manson, Pan European LPQI power quality survey, in: 19th International Conference on Electricity Distribution (CIRED), Vienna, 2007.
[6] J.Y. Chan, J.V. Milanovic, Risk based assessment of financial losses due to voltage sag, IEEE Trans. Power Deliv. 26 (2011).
[7] "JWG CIGRE-CIRED C4.107," in: Economic Framework for Power Quality (2010).
[8] J. Hughes, The integrated energy and communication systems architecture volume II, in: Permanent Power Quality Measurement, Electric Power Research Institute (EPRI), Palo Alto, CA, 2004.
[9] CEER, 5th CEER Benchmarking Report on the Quality of Electricity Supply, CEER, Brussels, 2011.
[10] M. Kezunovic, Smart Fault Location for Smart Grids, IEEE Trans. Smart Grid 2 (2011) 11–22.
[11] Y. Liao, Fault location for single-circuit line based on bus impedance matrix utilizing voltage measurements, IEEE Trans. Power Deliv. 23 (2008) 609–617.
[12] Y. Liao, Fault location observability analysis and optimal meter placement based on voltage measurements, Electric Power Syst. Res. 79 (2009) 1062–1068.
[13] N. Kang, Y. Liao, Double-circuit transmission-line fault location with the availability of limited voltage measurements, IEEE Trans. Power Deliv. 27 (2012) 325–336.
[14] G. Olguin, Voltage Dip (Sag) Estimation in Power Systems based on Stochastic Assessment and Optimal Monitoring, Department of Energy and Environment, Chalmers University of Technology, Goteborg, 2005.
[15] J.V. Milanović, C.P. Gupta, Probabilistic assessment of financial losses due to interruptions and voltage sags – Part II: practical implementation, IEEE Trans. Power Deliv. 21 (2006).
[16] J.V. Milanović, C.P. Gupta, Probabilistic assessment of financial losses due to interruptions and voltage sags – Part I: the methodology, IEEE Trans. Power Deliv. 21 (2006) 918–924.
[17] K. Li, State Estimation for power distribution systems and measurement impacts, IEEE Trans. Power Syst. 11 (1996) 911–916.
[18] Siemens, 9610 Power Quality Meter, 2011.
[19] R. Singh, B.C. Pal, R.A. Jabr, Distribution system state estimation through Gaussian mixture model of the load as pseudo-measurement, IET Gener. Transm. Distrib. 4 (2009) 50–59.
[20] R. Singh, B.C. Pal, R.B. Vinter, Measurement placement in distribution system state estimation, IEEE Trans. Power Syst. 24 (2009).
[21] J. Zhu, D.L. Lubkeman, A.A. Girgis, Automated fault location and diagnosis on electric power distribution feeders, IEEE Trans. Power Deliv. 12 (1997).
[22] Y. Zhang, J.V. Milanovic, Voltage sag cost reduction with optimally placed FACTS devices, in: 9th International Conference on Electrical Power Quality and Utilisation, Barcelona, 2007.
[23] N.C. Woolley, J.V. Milanovic, Estimating the Voltage Unbalance Factor Using Distribution System State Estimation, in: Innovative Smart Grid Technologies Europe, Gothenburg, Sweden, 2010.
[24] J. Shawe-Taylor, N. Christianini, Kernel Methods for Pattern Analysis, Cambridge University Press, 2004.